

# Squeeze dispersion and the effective diapycnal diffusivity of oceanic tracers

**Gregory L Wagner<sup>1</sup>, Glenn Flierl<sup>1</sup>, Raffaele Ferrari<sup>1</sup>, Gunnar Voet<sup>2</sup>, Glenn S Carter<sup>3</sup>, Matthew H Alford<sup>2</sup>, and James B Girton<sup>4</sup>**

<sup>5</sup>Earth, Atmospheric, and Planetary Sciences, Massachusetts Institute of Technology, Cambridge, MA

<sup>6</sup>Scripps Institution of Oceanography, University of California, San Diego, La Jolla, CA

<sup>7</sup>Department of Oceanography, University of Hawai'i at Manoa, Honolulu, HI

<sup>8</sup>Applied Physics Laboratory, University of Washington, Seattle, WA

## Key Points:

- Squeezing and stretching of density layers modulates the diapycnal diffusion of oceanic tracers
- Squeeze dispersion modulates dispersion across some isopycnals in the abyssal Samoan Passage
- Diapycnal transport is strongly affected by positive correlations between squeezing and turbulence

**Abstract**

We describe a process called ‘squeeze dispersion’ in which the squeezing of oceanic tracer gradients by waves, eddies, and bathymetric flow modulates diapycnal fluxes by centimeter to meter-scale turbulence. Due to squeeze dispersion, the average effective diapycnal diffusivity of oceanic tracers is different and typically greater than the average ‘local’ diffusivity, especially when local diffusivity correlates with squeezing. We develop a theory to quantify the effects of squeeze dispersion on diapycnal oceanic transport, finding formulas that connect density-average tracer flux, locally-measured diffusivity, large-scale oceanic strain, the thickness-weighted average buoyancy gradient, and the effective diffusivity of oceanic tracers. We use this effective diffusivity to interpret observations of abyssal flow through the Samoan Passage reported by Alford et al. (2013) and find that squeezing modulates diapycnal tracer dispersion by factors between 0.5 and 3.

**Plain language summary**

Turbulent vertical ocean mixing is a crucial part of the Earth’s climate system, drawing atmospheric carbon and heat into the massive reservoir that is the deep ocean. Quantifying vertical ocean mixing is difficult: vertical mixing is associated with turbulence at the tiny scales of centimeters to meters, but affects the entire ocean on the long time scales of decades and centuries. We demonstrate that vertical ocean mixing depends not *only* on small scale turbulence as previously thought, but on the *combination* of small scale turbulence and larger scale motions, such as currents, eddies and waves similar to the jet streams and hurricanes of the atmosphere. In particular, when a patch of ocean is mixed by small-scale turbulence while being ‘squeezed’ in the vertical at the same time by currents and eddies, the patch ultimately mixes more quickly than the turbulence would cause alone. This means that estimating the total rate of oceanic vertical mixing requires knowledge both of the magnitude of ocean squeezing as well as the intensity of small scale ocean turbulence.

41

**1 Introduction**

Squeeze dispersion is a process in which the diapycnal diffusion of tracers such as dissolved carbon, temperature, salinity, oxygen, nutrients, and plankton is modulated in fluctuating flows that alternately squeeze material surfaces together and stretch them apart. Squeeze dispersion is a non-turbulent process relevant to flows that have moderate strain, but lack the crinkling, rolling up, and exponential stretching of material surfaces associated with turbulent mixing. Squeeze dispersion plays a role in flows under strong geometric or dynamical constraints: for example, low Reynolds flows confined by solid boundaries, or stratified, rotating, and anisotropic planetary flows.

In this paper we explore the effect of squeeze dispersion on transport across density surfaces in Earth’s ocean, where strong stratification and rotation limits turbulent mixing to ‘microscales’ smaller than approximately ten meters. Where a wide scale separation between microscale mixing and ‘macroscale’ flows with vertical scales of ten to thousands of meters exists, diapycnal fluxes are, from perspective of macroscale flows, approximately diffusive and characterized by an inhomogeneous and isotropic local diffusivity,  $\kappa$ . Macroscale flows associated with strain and squeeze dispersion include mesoscale and submesoscale eddies, fronts, and large-scale internal waves.

An estimate for the vertical diffusive flux across a squeezed macroscale layer of fluid illustrates the basic mechanism of squeeze dispersion. In this scenario, depicted in figure 1, a layer of fluid bound between material and isotracer surfaces with concentrations  $c$  and  $c+\Delta c$  is squeezed and stretched by a macroscale flow with strain but no overturning. Mi-

63 croscale turbulent mixing across the layer associated with overturning on scales much smaller  
 64 than the separation between the two surfaces is characterized by the vertical diffusive flux  
 65  $F = -\kappa \Delta c / h$ , where  $\kappa$  is the isotropic turbulent diffusivity and  $h$  is the vertical separa-  
 66 tion between the surfaces.

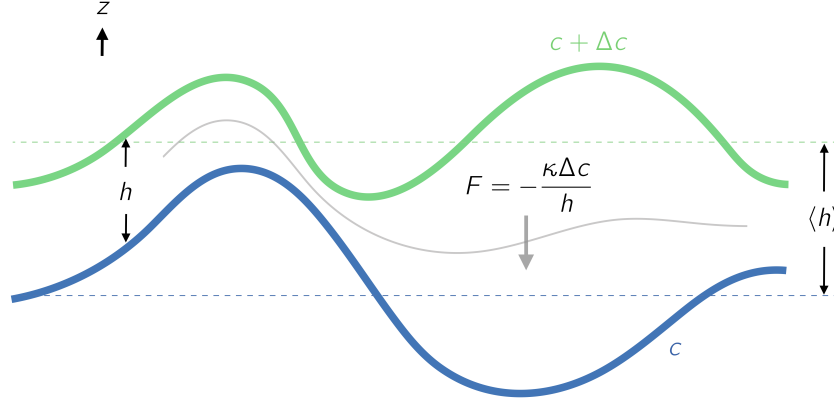


Figure 1: Squeeze dispersion between two isotracer surfaces with tracer concentrations  $c$  and  $c + \Delta c$ . The diffusive flux between the fluctuating surfaces is  $F = -\kappa \Delta c / h$ , where  $h$  is the separation between the surfaces and  $\kappa$  is the local diffusivity across the layer. The spatially-averaged separation between the two surfaces is  $\langle h \rangle$ . Introducing an effective squeeze dispersion diffusivity  $\kappa_e = \langle h \rangle (\kappa / h)$  implies that  $\langle F \rangle = -\kappa_e \Delta c / \langle h \rangle$ .

The average vertical tracer flux across the layer is  $\langle F \rangle = -\Delta c \langle \kappa / h \rangle$ , where the angle brackets denote an average that follows the motion of the layer and encompasses fluctuations in both  $h$  and  $\kappa$ . This formula for  $\langle F \rangle$  reflects the intuitive fact that, relative to a fixed  $\kappa$  distribution, an increase in squeezing and thus variations in  $h$  acts to increase the average flux  $\langle F \rangle$  across the layer. Increasing diffusive flux with increasing strain is the hallmark of squeeze dispersion. To express  $\langle F \rangle$  in terms of the average separation between the surfaces  $\langle h \rangle$  we introduce the effective diffusivity,

$$\kappa_e = \langle h \rangle \left\langle \frac{\kappa}{h} \right\rangle, \quad (1)$$

such that  $\langle F \rangle = -\kappa_e \Delta c / \langle h \rangle$ .

The squeeze dispersion effective diffusivity in (1) is simple quantification of the effects of the squeeze dispersion process that depends on an average that follows the vertical motion of a strained layer of fluid. The squeeze dispersion process itself does not, however, depend on the averaging method — Lagrangian, Eulerian, or otherwise — used to quantify its effect. To make this point concrete, we introduce an example in section 2 that illustrates squeeze dispersion in the advection of a tracer patch over undulating bathymetry by a spatially-variable, squeezing and stretching barotropic flow. In this example, the effective diffusivity in (1) arises in the exact analytical solution to the barotropic squeezing problem. In section 3, we show further that the effective diffusivity (1) arises in the thickness-weighted-average equation (9) for the dispersion of tracers on the scales of ocean circulation alongside the familiar processes of advection by the residual-mean circulating velocity and isopycnal diffusive mixing by mesoscale eddies.

The effective diffusivity (1) is a bulk diffusivity obtained by averaging tracer flux over macroscale fluctuations and along isopycnals and dividing the result by the thickness-weighted-average tracer gradient. This interpretation of (1) in terms of tracer fluxes suggests a method

83 for analyzing microstructure observations that makes use of Osborn (1980)'s hypothesized  
 84 relationship between turbulent dissipation rate and buoyancy flux: rather than 'averaging  
 85  $\kappa$ ', the computation of (1) requires averaging the buoyancy flux  $\Gamma\epsilon$  along surfaces or layers  
 86 of constant density, where  $\Gamma$  is the mixing coefficient, the proportionality constant be-  
 87 tween turbulent dissipation rate  $\epsilon$  and local buoyancy flux.

88 In section 4, we implement this method for calculating  $\kappa_e$  in (1) in an analysis of mi-  
 89 crostructure observations from the Samoan Passage, and find that the effective diapycnal  
 90 diffusivity of tracers advected through the Samoan passage differs from the isopycnal-averaged  
 91 local diffusivity by factors of 0.5–3. This difference between bulk effective diffusivity and  
 92 average local diffusivity in the Samoan passage suggests that realistic variations in diffusiv-  
 93 ity and squeezing can cause substantial modulation in the dispersion of oceanic tracers. The  
 94 difference between average diffusivity and effective squeeze dispersion diffusivity may con-  
 95 tribute to differences between tracer-based and microstructure-based estimates of diapyc-  
 96 nal diffusivity inferred from observations as, for example, in the Brazil Basin (Ledwell et  
 97 al., 2000), the east Pacific sector of the Antarctic Circumpolar Current (Ledwell, St. Lau-  
 98 rent, Girton, & Toole, 2011), and Drake Passage (Mashayek et al., 2017; St. Laurent et  
 99 al., 2012; Watson et al., 2013).

## 100 2 Squeeze dispersion in flow over undulating bathymetry

101 The squeeze dispersion process is illustrated by the advection of a diffusing tracer patch  
 102 through the contracting streamlines of a two-dimensional flow  $u(x), w(x, z)$ . This exam-  
 103 ple may be alternatively interpreted as mid-depth tracer dispersion in a barotropic shallow  
 104 water flow with rigid lid and undulating bathymetry, or as the advection of a tracer patch  
 105 between two isopycnals in a slowly-varying, large-scale straining flow.

In either interpretation, the effects of microscale turbulent mixing are modeled by an inhomogeneous turbulent diffusivity,  $\kappa(x, z, t)$ . The tracer concentration  $c(x, z, t)$  then obeys the advection-diffusion equation

$$c_t + uc_x + wc_z = \partial_x(\kappa c_x) + \partial_z(\kappa c_z), \quad (2)$$

where the barotropic horizontal and vertical velocity are

$$u(x) = \frac{U}{H} \quad \text{and} \quad w(x, z) = \frac{zUH_x}{H^2}, \quad (3)$$

with barotropic transport  $U$ , length  $L$ , depth

$$H(x) = \langle H \rangle [1 - a \sin(\frac{2\pi x}{L})], \quad (4)$$

average depth  $\langle H \rangle$ , and non-dimensional relative bathymetric height  $a$ .

Figure 2(a) shows a time lapse of the evolution of an initially Gaussian tracer patch with  $\int c dx dz = 1$  squeezed and stretched by the flow in (3) with constant  $\kappa$ . We compare the prescribed  $\kappa$  to the measured effective diffusivity  $\kappa_e = (2T)^{-1} \int (Z-z)^2 c dx dz$ , where  $Z = \int z c dx dz$  is the z-centroid of the tracer patch, based on the change in the vertical variance of the tracer patch over the interval  $T = \langle H \rangle L/U$  during which the patch travels from  $x = 0$  to  $x = L$ . This definition of  $\kappa_e$ , introduced by Aris (1956), is used to interpret oceanic tracer release experiments such as that reported by Ledwell et al. (2011). In figure 2(b), the ratio between the numerically measured effective diffusivity  $\kappa_e$  and the prescribed constant diffusivity  $\kappa$  is plotted with purple circles, showing how squeeze dispersion always increases  $\kappa_e$  over a constant  $\kappa$ . This is squeeze dispersion: tracer dispersion increases with increasing  $a$  and thus increasing squeezing, despite acceleration of the tracer patch over the constriction and stretching over the contraction.

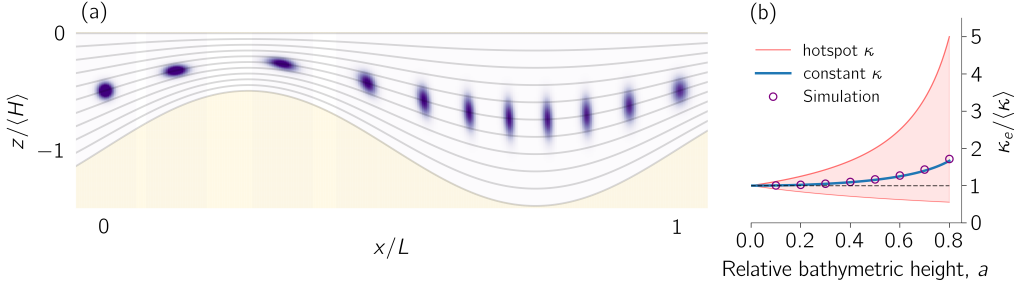


Figure 2: (a) Time-lapse of tracer patch advection in a numerical solution to (2)–(4) with  $a = 0.5$ . (b) Modulation of diffusion by squeeze dispersion in a numerical solution to (2)–(4) (purple circles) with constant  $\kappa$ , the theoretical prediction 6 with constant  $\kappa$  (blue line), and the theoretical prediction for mixing ‘hotspots’ located at the point of maximum squeezing ( $\kappa \propto \delta(x + L/4)$ , upper red line) and the point of maximum stretching ( $\kappa \propto \delta(x + 3L/4)$ , lower red line). Red shading indicates the range of possible modulation of diffusion by squeezing in this problem and a grey dashed line indicates  $\kappa_e/\langle \kappa \rangle = 1$ . We use  $U = 1$ ,  $\langle H \rangle = 1$ ,  $L = 20$ ,  $\kappa = 10^{-4} \text{ m}^2 \text{s}^{-1}$  and tracer initial condition  $c(t=0) = \exp[-x^2/2\ell^2 - (z + \langle H \rangle/2)^2/2d^2]/2\pi\ell d$  with  $\ell = L/100$  and  $d = \langle H \rangle/20$ .

The nature of this enhancement in dispersion is revealed by a special solution to (2)–(3) derived in appendix A in which we assume the tracer patch has a thin aspect ratio such that  $\partial_x(\kappa c_x) \ll \partial_z(\kappa c_z)$ , use a transformation into bathymetric coordinates with the initial condition  $c(t=0) = \delta(x)\delta(z+\langle H \rangle/2)$ , and allow turbulent diffusivities of the form  $\kappa(x, t)$ . The tracer distribution in this solution is tellingly Gaussian after being advected for a time  $t_n = n\langle H \rangle L/U$  through  $n$  ‘squeezing cycles’ over the periodic bathymetry,

$$c(t=t_n) = \frac{1}{\sqrt{4\pi\kappa_e t_n}} \exp\left[-\frac{(z+\langle H \rangle/2)^2}{4\kappa_e t_n}\right] \delta(x-nL), \quad (5)$$

and therefore spreads diffusively in the vertical while advected horizontally. However, rather than spreading with the trajectory-averaged diffusivity, for example, the effective diffusivity that determines tracer patch dispersion is

$$\kappa_e = \langle H \rangle \left\langle \frac{\kappa}{H} \right\rangle, \quad \text{where} \quad \langle \phi \rangle \stackrel{\text{def}}{=} \frac{1}{L} \int_0^L \phi dx. \quad (6)$$

119  $\kappa_e$  in (5)–(6) is identical to the effective diffusivity defined in terms of the growth of tracer 120 variance,  $\kappa_e = (2T)^{-1} \int (Z-z)^2 c dx dz$ . Because  $\langle 1/H \rangle \geq 1/\langle H \rangle$  for any positive function  $H(x)$ , (6) implies that fluctuating squeezing always enhances the diffusive transport 121 associated with a constant  $\kappa$ . Moreover, the enhancement is increased further relative to 122  $\langle \kappa \rangle$  when  $\kappa$  and squeezing positively correlate. 123

124 In figure 2(b) we compare the diffusivity modulation  $\kappa_e/\langle \kappa \rangle$  in numerical solutions 125 to (2) (purple circles) with the theoretical prediction (6) (blue line) versus  $a$ . The numerical 126 and analytical solutions show that  $\kappa_e/\langle \kappa \rangle > 1$  for constant  $\kappa$ , corresponding to a modest 127 enhancement in tracer diffusion due to squeeze dispersion. The slight disagreement between 128 the numerical and analytical solutions for constant  $\kappa$  is due to the contribution of horizontal 129 diffusion and shear to the vertical dispersion of the patch in the numerical solution. The 130 red solid lines plot (6) for diffusivity ‘hot spots’ associated with  $\kappa \propto \delta(x - L/4)$  (upper red line) and  $\kappa \propto \delta(x - 3L/4)$  (lower red line) that form upper and lower 131

132 bounds for the modulation of  $\kappa_e$  due to squeeze dispersion, showing how correlations be-  
 133 tween squeezing and a non-constant  $\kappa$  can act to either reduce or significantly enhance the  
 134 tracer effective diffusivity  $\kappa_e$  relative to  $\langle \kappa \rangle$ .

### 135 3 Effect of squeeze dispersion on the circulation of oceanic tracers

136 In this section we show that squeeze dispersion affects the diapycnal diffusion of trac-  
 137 ers on the scales of ocean circulation in continuous, depth-dependent stratification and flow.  
 138 For this we use a series of two averages introduced by both De Szeoke and Bennett (1993)  
 139 and Young (2012) to obtain a description of circulation-scale oceanic tracers that distin-  
 140 guishes between advection by the residual-mean circulation, isopycnal dispersion by mesoscale  
 141 eddies, and diapycnal squeeze dispersion by microstructure turbulence.

We first apply a spatial ‘microscale average’ over turbulent fluctuations and density inversions on scales of centimeters to  $O(10)$  meters. The microscale average (*i*) yields a monotonic density field and enables the use of buoyancy coordinates, and (*ii*) permits the turbulent closure  $\tilde{\mathbf{u}}\tilde{c} = -\kappa\nabla c$  for the average microscale turbulent flux  $\tilde{\mathbf{u}}\tilde{c}$ , where  $\tilde{\mathbf{u}}$  is the microscale velocity field,  $\tilde{c}$  is the microscale tracer concentration,  $\kappa$  is the microscale turbulent diffusivity and  $\nabla c$  is the ‘macroscale’ tracer gradient. The macroscale tracer concentration  $c$  then obeys

$$c_t + \mathbf{u} \cdot \nabla c = \nabla \cdot (\kappa \nabla c), \quad (7)$$

142 where the advecting velocity field  $\mathbf{u}$  includes large scale internal waves as well as subme-  
 143 soscale, quasi-geostrophic, and bathymetric flows with vertical scales larger than 10 me-  
 144 ters.

We introduce a second, thickness-weighted ‘macroscale average’ defined for any variable  $\phi$  via

$$\hat{\phi} \stackrel{\text{def}}{=} \frac{\langle h\phi \rangle}{\langle h \rangle}. \quad (8)$$

145 In (8),  $h \stackrel{\text{def}}{=} g/b_z$  is the ‘thickness’ of the buoyancy surface  $b = -gp'/\rho_0$ , where  $g$  is grav-  
 146 itational acceleration,  $\rho_0$  is a reference potential density, and  $p'$  is the potential density per-  
 147 turbation therefrom. The angle brackets in (8) denote an ensemble, time, or spatial av-  
 148 erage over macroscale fluctuations in buoyancy coordinates (Young, 2012). Though our  
 149 results are strictly true only for ensemble averages, time or spatial averages may be used  
 150 to similar but approximate effect where ensembles of oceanic motion are not available (Davis,  
 151 1994). Averaging in buoyancy coordinates is crucial for distinguishing between fundamen-  
 152 tal circulation processes: advection of tracer by the residual velocity, stirring of tracers along  
 153 mean isopycnal surfaces by mesoscale eddies, and mixing across mean density surfaces by  
 154 microscale turbulence.

We show in appendix B that applying the thickness-weighted average in (8) to the macroscale tracer equation (7) leads to an equation for the evolution of tracers on the scales of ocean circulation:

$$\left( \partial_t + \mathbf{u}^{\#} \cdot \nabla - \partial_z \langle h \rangle \underbrace{\left\langle \frac{\kappa}{h} \right\rangle}_{\stackrel{\text{def}}{=} \kappa_e} \partial_z \right) \hat{c} = -\nabla \cdot \mathbf{E}^c. \quad (9)$$

155 Equation (9) describes the dispersion of the large-scale tracer concentration  $\hat{c}$  due to ad-  
 156 vection by the circulation velocity  $\mathbf{u}^{\#}$ , stirring and diffusion by macroscale eddy fluxes  $\mathbf{E}^c$   
 157 defined in (B.14), and across-isopycnal diffusion due to the effective diapycnal diffusivity  
 158  $\kappa_e = \langle h \rangle \langle \kappa/h \rangle$ .

159 Ocean models that employ the Gent and Mcwilliams (1990) scheme to parameter-  
 160 ize mean advection by mesoscale eddies and the Redi diffusivity (Redi, 1982) to parame-  
 161 terize eddy mixing along isopycnals may implicitly use (9) to model the dispersion of oceanic

162 tracers (McDougall & McIntosh, 2001). In these models, the Redi diffusivity acts to pa-  
 163 rameterize the eddy fluxes  $\mathbf{E}^c$  in (9), while the advecting velocity field  $\mathbf{u}^\#$  is modeled as  
 164 the sum of a resolved velocity field and a ‘quasi-Stokes’ velocity field (McDougall & McIn-  
 165 tosh, 2001) approximated by the Gent and Mcwilliams (1990) scheme. In these models and  
 166 in actuality, isopycnal advection and mixing dominate the isopycnal dispersion of oceanic  
 167 tracers at large scales. Equation (9) demonstrates how diapycnal squeeze dispersion com-  
 168 plements isopycnal mixing by eddy fluxes  $\mathbf{E}^c$  and residual advection by  $\mathbf{u}^\#$  to determine the  
 169 total — along-isopycnal and cross-isopycnal — dispersion of oceanic tracers.

170 The effective diapycnal diffusivity experienced by oceanic tracers is given by the squeeze  
 171 dispersion formula  $\kappa_e = \langle h \rangle \langle \kappa/h \rangle$ , directly analogous to the effective diffusivity (6) that  
 172 emerges in the parameterization in the introduction and the barotropic problem in section 2.  
 173 The coarse-grained argument developed in the introduction thus translates to cases with  
 174 continuous stratification and flow, in which advection by vertically convergent and diver-  
 175 gent flows acts to increase and decrease vertical tracer gradients. The mediation of oceanic  
 176 tracer diffusion by squeeze dispersion implies an outsized importance for correlations either  
 177 dynamical or coincidental between squeezing and microscale turbulence.

#### 178 4 Squeeze dispersion in the Samoan Passage

179 To evaluate the effect of squeeze dispersion in observed oceanic scenarios, we com-  
 180 pare the effective squeeze diffusivity in (1) and (9) with the average local diffusivity of a  
 181 hypothetical tracer advected along isopycnals in observations of abyssal flow through the  
 182 Samoan Passage — a 40 km-wide conduit between the southern and northern Pacific Ocean  
 183 where strong abyssal flow over rough and constricted bathymetry produces hydraulic jumps,  
 184 lee waves, turbulence, and squeezing. We focus on the eastern channel of the Samoan Pas-  
 185 sage using a series of hydrographic and direct turbulence observations made in 2012 sum-  
 186 marized in figure 3(a) and by Alford et al. (2013).

187 Our analysis uses 13 vertical profiles of small-scale shear, temperature, and pressure  
 188 made by a Rockland Vertical Microstructure Profiler (VMP). The location of the 13 VMP  
 189 profiles are overlaid over contours of Samoan passage bathymetry in figure 3(a). Because  
 190 conductivity was not measured by the VMP, we estimate VMP salinity with a 5th-order poly-  
 191 nomial fit to the temperature-salinity relationship measured by nearby Sea-Bird 911plus Conductivity-  
 192 Temperature-Depth (CTD) profiles. The temperature, conductivity, and pressure profiles  
 193 are processed to produce 1 meter gridded data and used to compute profiles of potential  
 194 density referenced to 4,000 meters, which we denote  $\sigma$ . The turbulent kinetic energy dis-  
 195 sipation rate,  $\epsilon \stackrel{\text{def}}{=} \nu |\nabla \tilde{\mathbf{u}}|^2$ , where  $\nu$  is the kinematic ocean viscosity and  $\tilde{\mathbf{u}}$  is the microscale  
 196 velocity field, is estimated from the VMP data by fitting local shear fluctuation spectra to  
 197 the Nasmyth spectrum (Oakey & Elliott, 1982) and further integrating following Gregg (1998).

198 We next define 22 layers equally distributed in density space between  $\sigma = 45.85 \text{ kg m}^{-3}$   
 199 and  $\sigma = 45.96 \text{ kg m}^{-3}$  with width  $\Delta\sigma = 0.005 \text{ kg m}^{-3}$ . The depth of these 22 density  
 200 layers ranges from 3144 to 5106 meters within the 13 VMP profiles. The gridded  $\sigma(z)$  pro-  
 201 files and 22 density layers  $\sigma_i \pm \frac{1}{2}\Delta\sigma$  are visualized in figure (3)(b).

The vertical extent of each density layer,  $\Delta\zeta_i$ , and layer-averaged turbulent dissipa-  
 tion,  $\epsilon_i$ , are computed for each profile by sorting the  $\sigma$  profile to obtain a monotonic, sta-  
 bly stratified density profile  $\sigma'(z)$  and permuting  $\epsilon$  to find  $\epsilon'$  such that  $\epsilon'(\sigma') = \epsilon(\sigma)$ . We  
 next invert  $\sigma'(z)$  to find  $\zeta' = z(\sigma')$ , where  $z$  is a vertical coordinate that increases up-  
 wards to  $z = 0$  at the ocean surface, and linearly interpolate  $\zeta'$  in  $\sigma'$  to determine  $\Delta\zeta_i$  via

$$\Delta\zeta_i = \zeta' (\sigma_i - \frac{1}{2}\Delta\sigma) - \zeta' (\sigma_i + \frac{1}{2}\Delta\sigma) . \quad (10)$$

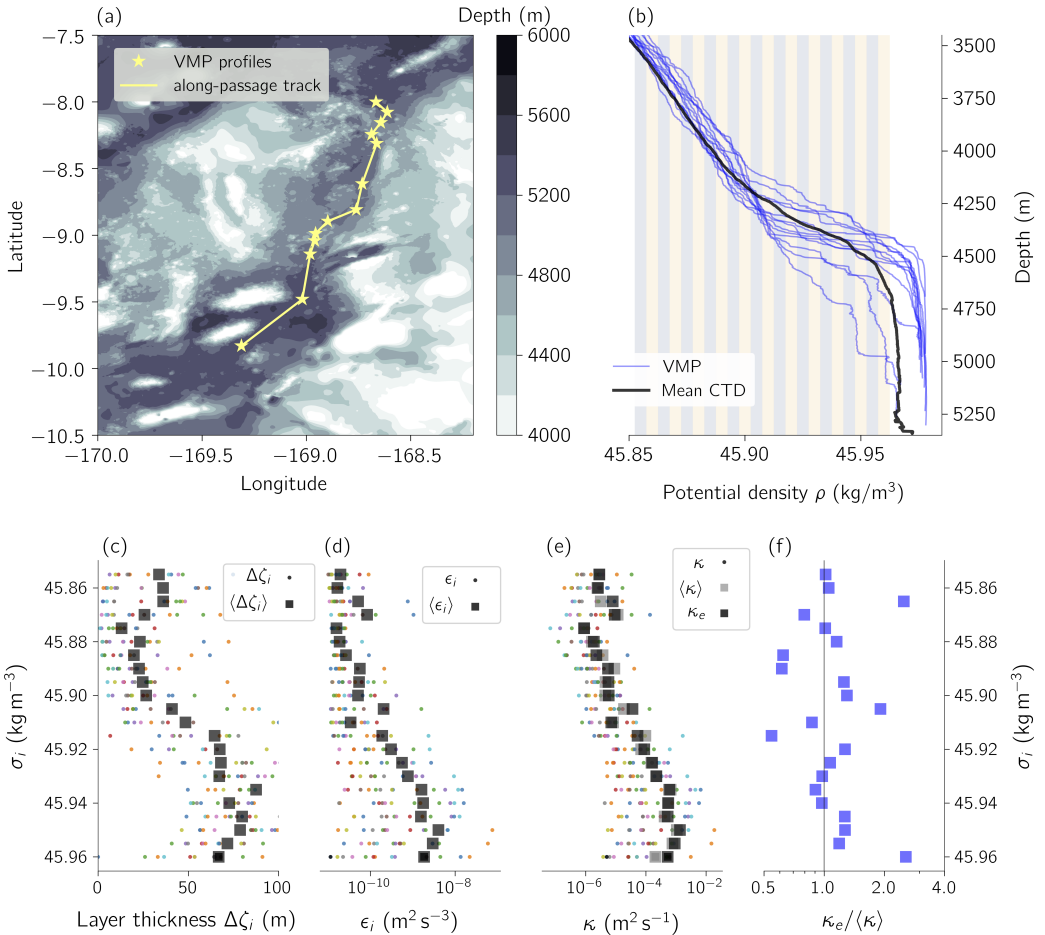


Figure 3: Effect of squeezing on diapycnal dispersion in the Samoan passage. (a) shows Samoan Passage bathymetry and VMP profile locations. (b) shows VMP density profiles in blue, the mean of 8 passage CTD density profiles in black, and the 22 density layers used for analysis with vertical stripes. (c), (d), and (e) show profiles and passage averages of layer thickness  $\Delta\zeta_i$ , layer-averaged turbulent dissipation rate  $\epsilon_i$ , and cross-layer diffusivity  $\kappa_i$ . (e) also plots effective diffusivity  $\kappa_e$  and (f) plots the ratio  $\kappa_e/\langle \kappa \rangle$ .

We compute the layer-averaged dissipation,  $\epsilon_i$ , from the sorted data by evaluating

$$\epsilon_i(\sigma_i) = \frac{1}{\Delta\sigma} \int_{\sigma_i - \Delta\sigma/2}^{\sigma_i + \Delta\sigma/2} \epsilon'(\sigma') d\sigma', \quad (11)$$

numerically with the trapezoidal rule and using linear interpolation in  $\sigma'$  to estimate  $\epsilon'$  at the end points  $\sigma_i \pm \frac{1}{2}\Delta\sigma$ . Finally, we note that the maximum overturn density adjustment  $\max(|\sigma' - \sigma|)$  over all profiles is  $0.0014 \text{ kg m}^{-3}$ , smaller than the layer size  $\Delta\sigma = 0.005$ .

We compute the local diffusivity across each density layer using Osborn (1980)'s formula for the relationship between turbulent dissipation and buoyancy flux,

$$\kappa(\sigma_i) \stackrel{\text{def}}{=} \frac{\Gamma\epsilon_i}{N_i^2}, \quad (12)$$

where  $\Gamma = 0.2$  is the mixing coefficient, the ratio between potential energy creation and kinetic energy dissipation. In (12),  $N_i^2$  is the buoyancy gradient across each  $\sigma_i$  layer defined in terms of  $\Delta\zeta_i$  via

$$N_i^2 = -\frac{g\Delta\sigma}{\rho_0\Delta\zeta_i}, \quad (13)$$

where  $g = 9.81 \text{ m s}^{-2}$  is gravitational acceleration and  $\rho_0 = 1045.85 \text{ kg m}^{-3}$ . (The specific values of  $g$  and  $\rho_0$  are irrelevant to the main conclusions of this section based on the ratio between effective diffusivity and local diffusivity.)

We develop a bulk average by defining an along-passage track that connects the 13 VMP stations with straight lines in latitude-longitude coordinates, and defining an along-passage coordinate 'x' that increases along the track from south to north. The along-passage track connecting VMP stations is shown in figure 3(a). We define an average of any variable  $\phi(x, \sigma_i)$  within a density layer  $\sigma_i$  and along the Samoan passage as

$$\langle \phi \rangle(\sigma_i) \stackrel{\text{def}}{=} \frac{1}{L} \int_0^L \phi(x, \sigma_i) dx, \quad (14)$$

where  $x$  is distance on the along-passage track in figure 3(a) and  $L$  is the total length of path connecting the VMP profiles. The integral in (14) is estimated from the discrete data using the trapezoidal rule. In Figure 3(c), (d), and (e), we compare the profiles and passage-averages of  $\Delta\zeta_i$ ,  $\epsilon_i$ , and  $\kappa$ , respectively.

We use (14) to compute the effective diffusivity in (1) and (9),  $\kappa_e = \langle h \rangle \langle \kappa/h \rangle$ , where the thickness is defined  $h = g/N^2$  in terms of the local buoyancy gradient  $N^2$  and gravitational acceleration  $g$ . This definition of the effective diffusivity with the average in (14) is reminiscent of the definition that appears in the effective diffusivity derived for the barotropic, 'single-layer' example in section 2. Inserting the formula for local diffusivity  $\kappa$  in (12) into the squeeze dispersion formula  $\kappa_e = \langle h \rangle \langle \kappa/h \rangle$  yields

$$\kappa_e(\sigma_i) = \left\langle \frac{1}{N_i^2} \right\rangle \langle \Gamma\epsilon_i \rangle. \quad (15)$$

$$= -\frac{\rho_0}{g\Delta\sigma} \langle \Delta\zeta_i \rangle \langle \Gamma\epsilon_i \rangle. \quad (16)$$

The ratio between the passage-averaged effective diffusivity (16) and the average local diffusivity,

$$\frac{\kappa_e}{\langle \kappa \rangle} = \frac{\langle \Delta\zeta_i \rangle \langle \epsilon_i \rangle}{\langle \Delta\zeta_i \epsilon_i \rangle}, \quad (17)$$

makes clear how substantial positive or negative correlations between turbulent mixing represented by  $\epsilon_i$  and squeezing represented by  $\Delta\zeta_i$  imply a substantial difference between turbulent buoyancy flux and the associated effective diffusivity, and the average local diffusivity. In other words,  $\kappa_e/\langle \kappa \rangle \geq 1$  implies a correlation between large  $\epsilon_i$  (mixing) and small  $\Delta\zeta_i$  (squeezing).

217 The layerwise effective diffusivity in (16) and ratio  $\kappa_e / \langle \kappa \rangle$  in (17) are plotted in figure  
 218 3(e) and (f).  $\kappa_e / \langle \kappa \rangle$  varies from 0.5–3, and is greater than unity more often than not.  
 219 The substantial discrepancy between the isopycnal-averaged local diffusivity and the effec-  
 220 tive squeeze diffusivity across some isopycnals implies that strain substantially affects to-  
 221 tal tracer dispersion in the Samoan passage.

## 222 5 Conclusions

223 ‘Squeeze dispersion’ is a process by which diapycnal strain modulates oceanic diapyc-  
 224 nal mixing. The importance of squeeze dispersion on net diapycnal mixing depends on (*i*)  
 225 the magnitude of oceanic vertical strain and squeezing and (*ii*) correlations between squeez-  
 226 ing and diapycnal turbulence. Squeezing is often weak in mesoscale oceanic flows, being  
 227 proportional to Rossby number in quasi-geostrophic flows or the nonlinearity of internal wave  
 228 fields. Yet plausible dynamical mechanisms may link mixing and strain: for example, squeez-  
 229 ing and intense turbulent mixing are co-located over mountainous bathymetry in the Samoan  
 230 Passage. Numerical simulations suggest that large-scale strain may enhance turbulent in-  
 231 tensity and mixing in preexisting shear layers (Kaminski, 2016). On the other hand, Alford  
 232 and Pinkel (2000) find a *negative* correlation between squeezing and turbulent overturns  
 233 and mixing in the near-surface ocean. Further observations and simulations are needed to  
 234 determine the relationship between oceanic strain and turbulent mixing throughout the wa-  
 235 ter column, especially where turbulence is strong and  $\kappa$  is large.

236 In section 3 we conduct an analysis of the effects of squeeze dispersion on tracer fluxes  
 237 across isopycnal surfaces with the thickness-weighted average that culminates in an expres-  
 238 sion for the effective diffusivity of the thickness-weighted average tracer distribution in (9).  
 239 The effective diffusivity does not necessarily describe the evolution of other average tracer  
 240 distributions. Take the Eulerian-average, for example: the Eulerian-average tracer flux due  
 241 to squeeze dispersion may include contributions both from the modified Eulerian-average  
 242 diffusive tracer flux and the Eulerian-average advective flux. Both of these are proportional  
 243 to  $\kappa$  in non-turbulent squeeze dispersion processes. In general, both the average tracer dis-  
 244 tribution and its effective diffusivity depend on whether the average is Eulerian or a thickness-  
 245 weighted average in buoyancy coordinates. We find that the Eulerian-average approach to  
 246 analyzing squeeze dispersion is more cumbersome and more difficult to interpret than the  
 247 relatively clear result of the thickness-weighted average approach used in section 3.

248 The squeeze dispersion effective diffusivity in (1) and (9) implies that the bulk dif-  
 249 fusivity of oceanic tracers is estimated by averaging turbulent buoyancy flux and dividing  
 250 by thickness-weighted-average buoyancy gradient. In section 4, we approximate the tur-  
 251 bulent buoyancy flux with  $\Gamma\epsilon$ , where  $\Gamma$  is the mixing coefficient and  $\epsilon$  is the turbulent ki-  
 252 netic energy dissipation rate. We then use the instantaneous buoyancy gradient  $N^2$  to es-  
 253 timate the thickness-weighted-average buoyancy gradient  $1/\langle 1/N^2 \rangle$ , so that the ratio be-  
 254 tween turbulent buoyancy flux and thickness-weighted-average buoyancy gradient expressed  
 by (1) and (9) becomes

$$\kappa_e = \left\langle \frac{1}{N^2} \right\rangle \langle \Gamma\epsilon \rangle , \quad (18)$$

255 where the angle brackets again denote an average in density space, or on an isopycnal. The  
 256 dependence of the effective squeeze dispersion diffusivity (18) on the average turbulent buo-  
 257 yancy flux  $\langle \Gamma\epsilon \rangle$  is consistent, for example, with the logic used by Voet et al. (2015) to com-  
 258 pare the average in-situ turbulent heat flux with a bulk estimate of heat flux from the tem-  
 259 perature distribution in the Samoan passage. In section 4, we develop a technique to coarse-  
 260 grain the Samoan passage observations reported in Alford et al. (2013) and Voet et al. (2015)  
 261 to evaluate equation (18) and interpret its implications for tracer dispersion.

255 Squeeze dispersion is not shear dispersion: squeeze dispersion is proportional to diffusivity while shear dispersion is inversely proportional to diffusivity. Squeeze dispersion requires velocity gradients parallel to the direction of dispersion, while shear dispersion requires only a velocity gradient perpendicular to the direction of the tracer dispersion. For example, vertical oceanic shear dispersion, which is negligible, is associated with lateral variations in vertical velocity and has an effect that is inversely proportional to lateral diffusivity. Vertical squeeze dispersion, on the other hand, persists under vanishing lateral diffusivity and is proportional to the strength of the vertical diffusivity.

263 The effective diffusivity for large-scale tracers in equation (1) and (9) implies that models  
264 that use the local diffusivity but do not fully resolve oceanic strain may underpredict oceanic  
265 tracer dispersion. In other words, the parameterization of diapycnal mixing in coarse res-  
266 olution models should take unresolved squeezing into account.

267 Finally, squeeze dispersion may also be important in other, non-oceanic laminar flows  
268 such as confined low Reynolds number flows. In these cases, the thickness  $h$  that appears  
269 in equation (1) and (9) should be interpreted as the separation between material sur-  
270 faces.

## 271 A Barotropic advection of tracer over bathymetry

Introducing the topographic coordinate  $\tilde{z} = z \langle H \rangle / H$ , where  $\langle H \rangle$  is a constant average depth and  $\langle \phi \rangle = L^{-1} \int_0^L \phi dx$  is the average of any quantity  $\phi$  over a tracer trajectory from  $x = 0$  to  $x = L$ , the tracer conservation equation (2) with flow field (3) transforms into

$$c_t + u c_x = \frac{\langle H \rangle^2 \kappa}{H^2} c_{\tilde{z}\tilde{z}}. \quad (\text{A.1})$$

In a coordinate frame following columns of fluid advected horizontally by the flow  $u = U/H$  with transport  $U$ , the vertical spread of the tracer is described by the deceptively ordinary equation

$$c_s = \langle \kappa \rangle c_{\tilde{z}\tilde{z}}, \quad (\text{A.2})$$

where  $\langle \kappa \rangle$  denotes the average values of  $\kappa$  over a trajectory. In (A.2),  $s$  is a time-like trajectory coordinate defined by

$$s(t) \stackrel{\text{def}}{=} \frac{\langle H \rangle^2}{\langle \kappa \rangle U} \int_{t_i}^t \frac{\kappa}{H} dt', \quad (\text{A.3})$$

where  $\kappa(x, t)$  and  $H(x)$  are evaluated along the column trajectory  $x = \xi(t)$ , which obeys  $\dot{\xi}_t = u(\xi)$ . The solution to (A.2) on short trajectories and with the initial condition  $c = \delta(\tilde{z} - \tilde{z}_0)\delta(x - x_0)$  is

$$c = \frac{1}{\sqrt{4\pi \langle \kappa \rangle s}} \exp \left[ -\frac{(\tilde{z} - \tilde{z}_0)^2}{4 \langle \kappa \rangle s} \right] \delta(x - \xi). \quad (\text{A.4})$$

272 The solution (A.4) is valid when the tracer concentration is negligible at the boundaries,  
273 which holds if the trajectory is short and the initial release point  $\tilde{z}_0$  is sufficiently far from  
274 the top or bottom. Evaluating (A.4) at  $t = \langle H \rangle L/U$  when the tracer patch reaches  $x = L$  yields equation (5).

## 276 B Derivation of the tracer circulation equation (9)

To derive the tracer circulation equation (9), we apply the thickness-weighted average defined in (8) to the macroscale tracer equation,

$$c_t + \mathbf{u} \cdot \nabla c = \nabla \cdot (\kappa \nabla c), \quad (\text{B.1})$$

277 first introduced in equation (7). We introduce the variable  $\varsigma \stackrel{\text{def}}{=} 1/b_z$  in this appendix for  
 278 convenience.  $\varsigma$  is related to the thickness  $h = g/b_z$  via  $\varsigma = h/g$  and corresponds to the  
 279 variable  $\sigma$  in Young (2012). In terms of  $\varsigma$  the thickness-weighted average in (8) is  $\hat{\phi} \stackrel{\text{def}}{=} \langle \varsigma \phi \rangle / \langle \varsigma \rangle$  for any variable  $\phi$ .  
 280

We first transform the macroscale tracer equation (B.1) from the Cartesian coordinates  $x, y, z, t$  to the buoyancy coordinates  $\tilde{x}, \tilde{y}, \tilde{b}, \tilde{t}$ . A thorough review of buoyancy coordinates is given by Young (2012). The material derivative  $D/Dt \stackrel{\text{def}}{=} \mathbf{u} \cdot \nabla c = u\partial_x + v\partial_y + w\partial_z$  in buoyancy coordinates is

$$\frac{D}{Dt} = u\partial_{\tilde{x}} + v\partial_{\tilde{y}} + \varpi\partial_{\tilde{b}}, \quad (\text{B.2})$$

where  $\varpi$  is the diabatic contribution to the buoyancy conservation equation such that  $D\bar{b}/Dt = \varpi$ . We define  $\varpi$  as

$$\varpi \stackrel{\text{def}}{=} \nabla \cdot (\kappa \nabla b), \quad (\text{B.3})$$

281 consistent with the diabatic contribution to the macroscale tracer equation (B.1). In other  
 282 words, we use a closure with turbulent diffusivity  $\kappa$  to approximate the effect of microstructure  
 283 fluxes for all tracers.

We simplify the microscale diabatic term  $\nabla \cdot (\kappa \nabla c)$  on the right side of (B.1) with two assumptions. First, we assume that buoyancy surfaces have small slopes and neglect terms proportional to  $\zeta_{\tilde{x}}$  or  $\zeta_{\tilde{y}}$ , where  $z = \zeta(\tilde{x}, \tilde{y}, \tilde{b}, \tilde{t})$  is the height of the buoyancy surface  $\tilde{b}$ . Second, we assume diffusive isopycnal tracer fluxes on circulation scales are dominated by macroscale stirring rather than microscale turbulence. We thus consider only the diabatic component of the diabatic flux, so that

$$\kappa \nabla c \approx \frac{\kappa C_{\tilde{b}}}{\varsigma^2} \mathbf{e}_3, \quad (\text{B.4})$$

284 where  $\mathbf{e}_3 = \mathbf{k}/\varsigma$  is the third covariant buoyancy-coordinate basis vector (Young, 2012) and  
 285  $\mathbf{i}, \mathbf{j}$ , and  $\mathbf{k}$  are the east, north, and vertical Cartesian coordinate unit vectors. Applying the  
 286 same assumptions to the diabatic buoyancy flux implies that  $\varpi \approx \varsigma^{-1} \partial_{\tilde{b}} (\kappa/\varsigma)$ .

We turn to the thickness-weighted average of the advection term  $Dc/Dt$  in (B.1). For any variable  $\phi$ , the thickness-weighted decomposition

$$\phi = \hat{\phi} + \phi'', \quad (\text{B.5})$$

defines the perturbation  $\phi''$ . A key identity derived by Young (2012) is

$$\left\langle \varsigma \frac{Dc}{Dt} \right\rangle = \langle \varsigma \rangle \left( \frac{D^\# \hat{c}}{Dt} + \nabla \cdot \mathbf{J}^c \right), \quad (\text{B.6})$$

where the residual material derivative

$$\frac{D^\#}{Dt} \stackrel{\text{def}}{=} \hat{u}\partial_x + \hat{v}\partial_y + w^\#\partial_z \quad (\text{B.7})$$

describes advection by the residual velocity field  $\mathbf{u}^\# = (\hat{u}, \hat{v}, w^\#)$ . The meaning of  $w^\#$  is described in the next paragraph. The perturbation flux in (B.6) is

$$\mathbf{J}^c \stackrel{\text{def}}{=} \widehat{u'' c''} \langle \mathbf{e}_1 \rangle + \widehat{v'' c''} \langle \mathbf{e}_2 \rangle + \widehat{\varpi'' c''} \langle \mathbf{e}_3 \rangle \quad (\text{B.8})$$

where the average basis vectors  $\langle \mathbf{e}_j \rangle$  are defined

$$\langle \mathbf{e}_1 \rangle \stackrel{\text{def}}{=} \mathbf{i} - \mathbf{k} b_x^\# / b_z^\#, \quad \langle \mathbf{e}_2 \rangle \stackrel{\text{def}}{=} \mathbf{j} - \mathbf{k} b_y^\# / b_z^\#, \quad \langle \mathbf{e}_3 \rangle \stackrel{\text{def}}{=} \mathbf{k} / b_z^\#. \quad (\text{B.9})$$

The vertical velocity  $w^\#$  in (B.7) and buoyancy field  $b^\#$  in (B.9) are defined in terms of the average depth of a buoyancy surface,  $\langle \zeta \rangle$ . In particular,  $b^\#$  is defined via  $z = \langle \zeta \rangle (\tilde{x}, \tilde{y}, b^\#, \tilde{t})$

and is therefore the value of the buoyancy surface whose mean position is  $x, t$ . The residual vertical velocity  $w^\#$ , on the other hand, is defined in terms of the motion of  $\langle \zeta \rangle$  via

$$w^\# \stackrel{\text{def}}{=} \frac{D^\# \langle \zeta \rangle}{Dt}. \quad (\text{B.10})$$

In this sense,  $w^\#$  and  $\langle \zeta \rangle$  have a similar relationship as  $w$  and  $\zeta$ . Neither  $w^\#$  nor  $b^\#$  are equal to their thickness-weighted counterparts  $\hat{w}$  and  $\hat{b}$ .

Turning back to the diabatic contribution on the right of (B.1), we use (B.4) and the identity  $\langle \varsigma \nabla \cdot \mathbf{F} \rangle = \nabla \cdot \hat{\mathbf{F}}^j \langle \mathbf{e}_j \rangle$  to obtain

$$\widehat{\nabla \cdot (\kappa \nabla c)} = \nabla \cdot \frac{\langle \kappa/\varsigma \rangle \hat{c}_b + \langle \kappa c''_b/\varsigma \rangle}{\langle \varsigma \rangle} \langle \mathbf{e}_3 \rangle. \quad (\text{B.11})$$

We then use  $\varpi = \varsigma^{-1} \partial_b (\kappa/\varsigma)$  to combine (B.11) with the divergence of the diapycnal term  $\widehat{\varpi'' c''} \langle \mathbf{e}_3 \rangle$  in (B.8) and transform the part of the result that depends on  $\hat{c}$  to Cartesian coordinates. When the dust settles, we find that

$$\nabla \cdot \widehat{(\varpi'' c'' - \kappa \nabla c)} \langle \mathbf{e}_3 \rangle = -\partial_z \left( \langle \varsigma \rangle \left\langle \frac{\kappa}{\varsigma} \right\rangle \partial_z \right) \hat{c} + \nabla \cdot \frac{\langle c'' \partial_b (\kappa/\varsigma) - \kappa c''_b/\varsigma \rangle}{\langle \varsigma \rangle} \langle \mathbf{e}_3 \rangle. \quad (\text{B.12})$$

The first term on the right of (B.12) describes the squeeze dispersion of  $\hat{c}$ , while the second term corresponds to the diabatic macroscale perturbation flux associated with the difference between the tracer distribution  $c$  and buoyancy distribution  $b$ .

We use (B.6) and (B.12) to write the thickness-weighted-average of (7):

$$\left( \partial_t + \mathbf{u}^\# \cdot \nabla - \partial_z \kappa_e \partial_z \right) \hat{c} = -\nabla \cdot \mathbf{E}^c, \quad (\text{B.13})$$

where  $\kappa_e \stackrel{\text{def}}{=} \langle h \rangle \langle \kappa/h \rangle = \langle \varsigma \rangle \langle \kappa/\varsigma \rangle$  and

$$\mathbf{E}^c \stackrel{\text{def}}{=} \widehat{u'' c''} \langle \mathbf{e}_1 \rangle + \widehat{v'' c''} \langle \mathbf{e}_2 \rangle + \langle \varsigma \rangle^{-1} \langle c'' \partial_b (\kappa/\varsigma) - \kappa c''_b/\varsigma \rangle \langle \mathbf{e}_3 \rangle. \quad (\text{B.14})$$

## Acknowledgments

Discussions with William R. Young, Jennifer MacKinnon, Carl Wunsch, Jim Ledwell, and Trevor MacDougall were helpful in writing this manuscript. GLW was supported by the NOAA Climate and Global Change Postdoctoral Fellowship Program, administered by UCAR's Cooperative Programs for the Advancement of Earth System Sciences. Samoan Passage research was funded by the National Science Foundation under grants OCE-1029268, OCE-1029483 and OCE-1657795. Julia code and notebooks to generate figures 2 and 3 can be found at <https://github.com/glwagner/SqueezeDispersionGRL>.

## References

- Alford, M. H., Girton, J. B., Voet, G., Carter, G. S., Mickett, J. B., & Klymak, J. M. (2013). Turbulent mixing and hydraulic control of abyssal water in the Samoan Passage. *Geophysical Research Letters*, 40(17), 4668–4674.
- Alford, M. H., & Pinkel, R. (2000). Observations of overturning in the thermocline: The context of ocean mixing. *Journal of Physical Oceanography*, 30(5), 805–832.
- Aris, R. (1956). On the dispersion of a solute in a fluid flowing through a tube. *Proc. R. Soc. Lond. A*, 235(1200), 67–77.

- 309 Davis, R. E. (1994). Diapycnal mixing in the ocean: Equations for large-scale budgets.  
310     *Journal of physical oceanography*, 24(4), 777–800.
- 311 De Szoeke, R. A., & Bennett, A. F. (1993). Microstructure fluxes across density sur-  
312     faces. *Journal of physical oceanography*, 23(10), 2254–2264.
- 313 Gent, P. R., & Mcwilliams, J. C. (1990). Isopycnal mixing in ocean circulation models.  
314     *Journal of Physical Oceanography*, 20(1), 150–155.
- 315 Gregg, M. (1998). Estimation and geography of diapycnal mixing in the stratified  
316     ocean. *Physical processes in lakes and oceans*, 305–338.
- 317 Kaminski, A. K. (2016). *Linear optimal perturbations and transition to turbulence in in-*  
318     *strongly-stratified shear flows* (Unpublished doctoral dissertation). University of  
319     Cambridge.
- 320 Ledwell, J., Montgomery, E., Polzin, K., Laurent, L. S., Schmitt, R., & Toole, J.  
321     (2000). Evidence for enhanced mixing over rough topography in the abyssal  
322     ocean. *Nature*, 403(6766), 179.
- 323 Ledwell, J., St. Laurent, L., Girton, J., & Toole, J. (2011). Diapycnal mixing in the  
324     Antarctic circumpolar current. *Journal of Physical Oceanography*, 41(1), 241–  
325     246.
- 326 Mashayek, A., Ferrari, R., Merrifield, S., Ledwell, J. R., St Laurent, L., & Garabato,  
327     A. N. (2017). Topographic enhancement of vertical turbulent mixing in the  
328     Southern Ocean. *Nature Communications*, 8, 14197.
- 329 McDougall, T. J., & McIntosh, P. C. (2001). The temporal-residual-mean velocity.  
330     part ii: Isopycnal interpretation and the tracer and momentum equations. *Journal*  
331     *of Physical Oceanography*, 31(5), 1222–1246.
- 332 Oakey, N., & Elliott, J. (1982). Dissipation within the surface mixed layer. *Journal of*  
333     *Physical Oceanography*, 12(2), 171–185.
- 334 Osborn, T. (1980). Estimates of the local rate of vertical diffusion from dissipation  
335     measurements. *Journal of Physical Oceanography*, 10(1), 83–89.
- 336 Redi, M. H. (1982). Oceanic isopycnal mixing by coordinate rotation. *Journal of Phys-*  
337     *ical Oceanography*, 12(10), 1154–1158.
- 338 St. Laurent, L., Naveira Garabato, A. C., Ledwell, J. R., Thurnherr, A. M., Toole,  
339     J. M., & Watson, A. J. (2012). Turbulence and diapycnal mixing in Drake  
340     Passage. *Journal of Physical Oceanography*, 42(12), 2143–2152.
- 341 Voet, G., Girton, J. B., Alford, M. H., Carter, G. S., Klymak, J. M., & Mickett, J. B.  
342     (2015). Pathways, volume transport, and mixing of abyssal water in the Samoan  
343     Passage. *Journal of Physical Oceanography*, 45(2), 562–588.
- 344 Watson, A. J., Ledwell, J. R., Messias, M.-J., King, B. A., Mackay, N., Meredith,  
345     M. P., ... Garabato, A. C. N. (2013). Rapid cross-density ocean mixing at mid-  
346     depths in the Drake Passage measured by tracer release. *Nature*, 501(7467),  
347     408.
- 348 Young, W. R. (2012). An exact thickness-weighted average formulation of the Boussi-  
349     nesq equations. *Journal of Physical Oceanography*, 42(5), 692–707.